

Local geometry around B atoms in B/Si(111) from polarized x-ray absorption spectroscopy

Saleem Ayaz Khan,¹ Martin Vondráček,² Peter Blaha,³ Kateřina Horáková,² Jan Minár,¹ Ondřej Šipr,⁴ and Vladimír Cháb²

¹*New Technologies Research Centre, University of West Bohemia,
Univerzitní 2732, 306 14 Pilsen, Czech Republic*

²*Institute of Physics ASCR v. v. i., Na Slovance 2, CZ-182 21 Prague, Czech Republic*

³*Institute of Materials Chemistry, TU Vienna, Getreidemarkt 9, A-1060 Vienna, Austria*

⁴*Institute of Physics ASCR v. v. i., Cukrovarnická 10, CZ-162 53 Prague, Czech Republic*

(Dated: November 29, 2021)

The arrangement of B atoms in a doped Si(111)-($\sqrt{3} \times \sqrt{3}$) $R30^\circ$:B system was studied using near-edge x-ray absorption fine structure (NEXAFS). Boron atoms were deposited via segregation from the bulk by flashing the sample repeatedly. The positions of B atoms are determined by comparing measured polarized (angle-dependent) NEXAFS spectra with spectra calculated for various structural models based on ab-initio total energy calculations. It is found that most of boron atoms are located in sub-surface L_1^c positions, beneath a Si atom. However, depending on the preparation method a significant portion of B atoms may be located elsewhere. A possible location of these non- L_1^c -atoms is at the surface, next to those Si atoms which form the ($\sqrt{3} \times \sqrt{3}$) $R30^\circ$ reconstruction.

Keywords: ab-initio; structure analysis; XAS;

I. INTRODUCTION

Studies of the B/Si(111) system started intensively in the late eighties^{1,2}. After a period of a declined interest, the research has again intensified stimulated by attempts to prepare a passivated Si surface in connection with the development of molecular electronics. Full introduction of molecules into the technology is still in its initial stages, related to a production of hybrid circuits composed of parts produced with Si-based and organic technologies. One of the challenges in this field is tailoring the interaction between deposited molecules and a substrate that is needed for wiring in a device. Employment of the B/Si(111) system is very promising as it can be prepared with different technologies (segregation or epitaxy) and with different properties: either as a spacer or as a passivated surface layer in the form of δ -doping. The latter one offers a surface with active isolated Si atoms that can be considered as centres for molecule

capturing. This view is supported, e.g., by a recent theoretical work concentrating on the interaction of various metalphthalocyanine (MPc) molecules with the δ -doped Si(111)-($\sqrt{3} \times \sqrt{3}$) $R30^\circ$:B surface: for some molecules this interaction has van der Waals character that enables diffusion of the molecules on the surface so that self-organized structures can be formed³.

The location of B atoms at the Si(111) surface was carefully examined in the past. Low-energy electron diffraction (LEED) and similar methods showed the common ($\sqrt{3} \times \sqrt{3}$) $R30^\circ$ surface where boron atoms might be located in the T or L_1^c positions⁴⁻⁶, well defined in the dimer-adatom-stacking fault model of the Si(111)- 7×7 surface. The most accepted position is the L_1^c site, with Si atoms on top of B atoms in the second layer. This conclusion has been supported by calculations of total energies for different structural models^{1,7-11}.

Despite the results obtained so far, the question where the B atoms are located cannot be regarded as settled.

The intensity of diffraction spots represents data averaged over different configurations that cannot be identified in detail. It is conceivable that local configurations that cannot be distinguished by the diffraction are present. Indeed, several local-probe studies involving scanning tunneling microscopy (STM) or atomic-force microscopy (AFM) suggest that the B atoms may occupy also other positions than the L_1^c site^{12–15}. A lot of attention was focused on how the structure varies depending on the conditions of preparation, especially on the heat treatment^{1,12–14,16,17}.

Recently a combined experimental (STM) and theoretical study showed that there can be two charge states and consequently two local L_1^c configurations for the δ -doped Si(111) surface owing to electron–lattice coupling¹⁸. One state corresponds to the ground state of the $(\sqrt{3} \times \sqrt{3})R30^\circ$ reconstruction while the second state is a two-electron bound state with an elevated Si adatom. The possibility of switching between these states has been found at low temperatures ($T < 70$ K). Note that the concept of two concurrent dynamically switchable geometries has been extensively employed in modelling the Si(100)- 2×1 reconstructed surface^{19–21}.

To learn more about the positions of B atoms at Si(111) it is desirable to employ a local method which, unlike the STM, probes a part of the sample large enough to be considered as truly representative. The x-ray absorption spectroscopy satisfies these needs: it is chemically specific, meaning that one can be sure that it is the nearest neighborhood of a B atom which is considered, and at the same time the area inspected is macroscopic (typically $0.1 \text{ mm} \times 0.5 \text{ mm}$). As concerns the theoretical approach, a potentially weak point of all previous studies is that they employed pseudopotentials. Such calculations are computationally efficient but a verification of the results by an all-electron method is always desirable.

In this study we present experimental near-edge x-ray absorption fine structure (NEXAFS) spectra measured at the B K -edge for boron δ -doped Si(111)- $(\sqrt{3} \times \sqrt{3})R30^\circ$

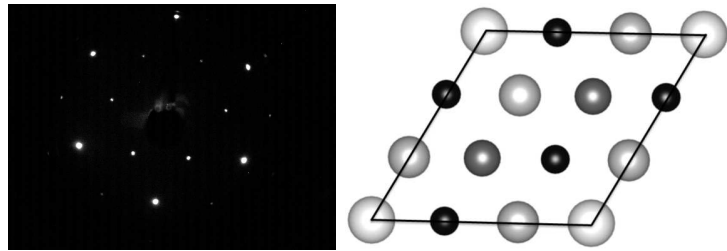


FIG. 1. (a) LEED of surface reconstruction $(\sqrt{3} \times \sqrt{3})R30^\circ$ for the B/Si(111) samples. (b) Schematic top view of the Si(111) $(\sqrt{3} \times \sqrt{3})R30^\circ$ reconstructed surface. Different size of atoms in different layers are used to provide a better insight.

surface, prepared by flashing at two different temperatures (1100°C and 900°C). The data are simulated using the all-electron WIEN2K code considering several trial geometries suggested by total energy minimization. By comparing experimental and theoretical NEXAFS spectra we found that the B atoms are mostly in the L_1^c positions. Depending on the preparation method, however, a significant portion of the B atoms may be in different positions, possibly in the surface L_1^a site, next to those Si atop atoms which form the $(\sqrt{3} \times \sqrt{3})R30^\circ$ reconstruction.

II. METHODOLOGICAL FRAMEWORK

A. Experiment

The samples were prepared by segregation of B atoms from the bulk: First, a clean Si surface was obtained by annealing a highly B-doped Si(111) wafer (resistivity less than $0.01 \text{ }\Omega\text{cm}$, $N_A \sim 10^{19} \text{ cm}^{-3}$) for 12 hours in ultra high vacuum at the temperature 500°C and pressure $8 \times 10^{-10} \text{ mbar}$. To achieve B atoms segregation, the samples were repeatedly flashed for 5 s at temperatures 1100°C (denoted as sample 1100) or 900°C (denoted as sample 900); the pressure was maintained less than $8 \times 10^{-9} \text{ mbar}$. After this procedure, a surface reconstruction $(\sqrt{3} \times \sqrt{3})R30^\circ$ has been identified by LEED,

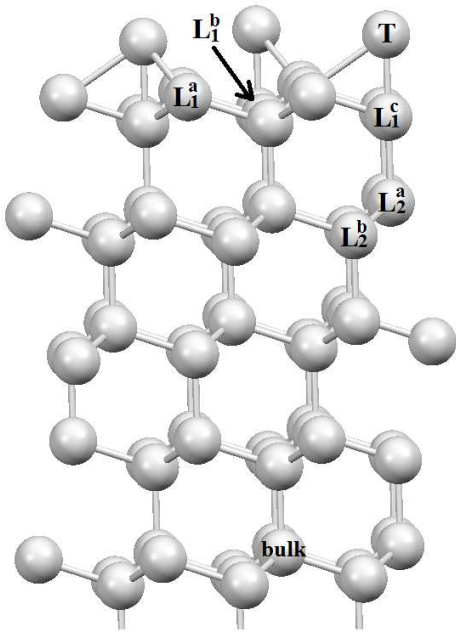


FIG. 2. Different configurations of the B atom at Si(111) $(\sqrt{3} \times \sqrt{3})R30^\circ$

as seen on Fig. 1(a).

B K -edge NEXAFS spectra were recorded at the Materials Science Beamline, Elettra Sincrotrone Trieste, Italy²². The data were acquired via surface sensitive Auger electron yield measurements, by recording the intensity of the B KLL Auger transition. The angle between the photon beam and the axis of the electron analyzer SPECS Phoibos 150 was fixed to 60° and the sample was rotated around the vertical axis. The NEXAFS spectra were acquired at four angles, ranging from normal incidence where the polarization vector ε is in the Si(111) (or xy) plane through the 30° incidence angle and normal emission angle (60° incidence) to the grazing incidence at 80° , with ε nearly parallel to the surface normal. The overall energy resolution for measured B K -edge NEXAFS spectra was 0.2 eV.

B. Structural models

The system is modeled by a supercell of slabs. Each slab consists of seven layers of Si atoms, with an addi-

tional incomplete layer of topmost Si atoms. Hydrogen atoms were added to saturate the dangling bonds at the other side of the slab. The thickness of the slab is about 23 Å. In the supercell the slabs are separated by about 14 Å of vacuum. Concerning the horizontal geometry, the slabs were constructed so that they correspond to the $(\sqrt{3} \times \sqrt{3})R30^\circ$ reconstruction which the B/Si(111) system undergoes (see the diagram in Figure 1(b)).

The structural models we explored were chosen by considering several positions of B atoms based on the ab-initio structural study of Andrade *et al.*¹¹. These positions are depicted schematically in Fig. 2, where we show five upper layers and the $(\sqrt{3} \times \sqrt{3})R30^\circ$ reconstruction atom at the top. We adopted a nomenclature that highlights the location of sites in specific layers, starting from the top (T , L_1 , L_2). Our study considers not only the L_1^c position (labeled as S5 by Andrade *et al.*¹¹) which attracted most attention in earlier works but also several other positions, which energetically least deviate from the L_1^c geometry and/or which should be considered based on kinematic reasons.

The structure relaxation was performed so that first the structure of bulk Si crystal was optimized to obtain the optimized bulk Si-Si distance (2.397 Å). This interatomic distance was then set as fixed for atoms in the two lowermost layers of our slab. The positions of the other atoms were optimized by allowing the atoms to move in the direction of the force until the equilibrium has been attained.

C. Calculations

The spectra were calculated by the ab-initio all-electron full potential linear augmented plane wave (FLAPW) method, as implemented in the WIEN2K code²³. The calculations were performed using the Perdew, Burke and Ernzerhof generalized gradient approximation (PBE-GGA) exchange-correlation functional²⁴. Additionally, we employed also the meta-

GGA SCAN functional²⁵ to evaluate the total energies for structures that have been already optimized via the PBE functional. This step is motivated by the fact that the SCAN functional often improves the energetics (while the atomic positions are usually well-predicted already with the PBE functional)²⁶.

Wave functions in the interstitial regions were expanded in plane waves, with the plane wave cutoff chosen so that $R_{\text{MT}}K_{\text{max}}=5$ (where R_{MT} represents the smallest atomic sphere radius and K_{max} is the magnitude of the largest wave vector). The R_{MT} radii were taken as 1.78 a.u. for Si atoms, 1.80 a.u. for B atoms and 0.95 a.u. for H atoms. The wave-functions inside the spheres were expanded in spherical harmonics up to the maximum angular momentum $\ell_{\text{max}}=10$. The \mathbf{k} -space integration was performed via a modified tetrahedron integration scheme. The internal geometry of the system is optimized using 2 \mathbf{k} -points in the irreducible Brillouin zone (IBZ) distributed according to a $(2 \times 2 \times 1)$ Monkhorst-Pack grid²⁷ while the self consistencies of the ground state energies were obtained by 8 \mathbf{k} -points in IBZ, distributed according to a $(4 \times 4 \times 1)$ Monkhorst-Pack grid.

Polarized x-ray absorption spectra were calculated via Fermi's Golden rule within the dipole approximation²⁸. The raw spectra were convoluted by a Gaussian with full width at half maximum (FWHM) of 0.3 eV and by a Lorentzian with FWHM of 0.2 eV, to simulate the effect of the experimental broadening and of the finite core hole lifetime. The differences between the NEXAFS for the $\varepsilon_{\parallel x}$ and $\varepsilon_{\parallel y}$ polarizations are very small, therefore we always display just their average. We distinguish in the following only between spectra with polarization vector in-plane (normal incidence) or out-of-plane (grazing incidence). There is a small difference between what is considered as grazing incidence in experiment and theory. In the experiments the grazing incidence means that the incoming radiation arrives at the sample not truly parallel to the surface but at an angle of 10° ; the polarization vector is thus tilted by 10° from the normal. In the cal-

culations we take the polarization vector exactly parallel to the surface normal. We do not expect any significant differences between spectra for the “true” and “approximative” grazing incidence setups.

The influence of the core hole on B K -edge NEXAFS can be considerable²⁹. It can be accounted for via one of the approximative static schemes. Frequently one relies on the final state rule³⁰, meaning that the spectrum is evaluated for electron states which have relaxed to the presence of the core hole. To employ this scheme, we performed first a self-consistent calculation with one $1s$ electron removed from the B atom and at the same time with one electron added to the valence states to maintain the charge neutrality. After the self-consistency had been achieved, another “single-shot” calculation was performed with the additional electron removed from the valence states, to get a proper Fermi level. We did not introduce another (larger) supercell scheme in this respect, because the B atoms are already quasi-isolated for the reconstructed $(\sqrt{3} \times \sqrt{3})R30^\circ$ system — their distance is 6.7 Å.

It is difficult to guess *a priori* which way of dealing with the core hole is the most suitable for a particular situation, therefore, we performed exploratory calculations for several core hole schemes: we calculated the NEXAFS (i) using a ground state potential (no core hole), (ii) using a potential obtained via the final state rule as described above and (iii) using a potential obtained via a final state rule with half of a core hole, which is equivalent to relying on Slater's transition state approximation. Following the outcome for one particular geometry (see appendix A), we decided to use the final state rule approximation with a full core hole throughout this study.

TABLE I. Total energies for systems with B atoms in positions depicted in Fig. 2. The values are given relative to the energy of the system with the B atom in the L_1^c position. Total energies of Andrade *et al.*¹¹ are shown for comparison (together with their notation for the positions of the B atoms).

position of B atom		ΔE (eV)		
notation	notation	PBE	SCAN	PBE
present	Andrade	present	present	Andrade
L_1^c	S5	0.00	0.00	0.00
L_2^a	B ₁	0.55	0.68	0.39
L_2^b	C	0.91	1.11	0.76
L_1^a	T ₅	1.14	1.31	1.05
L_1^b	A	1.18	1.25	1.21
T	T ₄	1.28	1.46	1.22
bulk	—	1.41	1.75	—

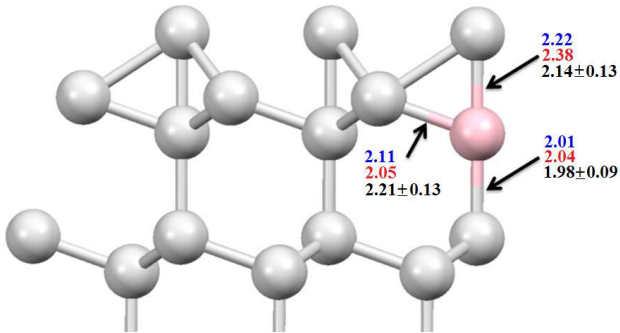


FIG. 3. Theoretical and experimental bond lengths of for B atom in the L_1^c position. The numbers stand for lengths in Å as obtained by the present work (top), by Andrade *et al.*¹¹ (middle), and by Baumgärtel *et al.*⁶ (bottom).

III. RESULTS

A. Comparing total energies

Total energies obtained for B atoms in positions depicted in Fig. 2 are presented in Tab. I. For comparison, we show also the results of earlier pseudopotential calculations of Andrade *et al.*¹¹. It follows from Tab. I that using the meta-GGA SCAN functional leads to the same trends as obtained for the GGA PBE functional — except for the L_1^a and L_1^b positions where the trend is reversed.

The calculations suggest that L_1^c is the favourable configuration. A detailed view on this configuration together with the bond lengths obtained from theory and LEED experiments⁶ is shown in Figure 3. There is a good agreement between the theoretical and experimental distances and in particular our all-electron results are always closer to experiment than the pseudopotential results of Andrade *et al.*¹¹.

B. Experimental and theoretical NEXAFS

Experimental B *K*-edge spectra for the sample 900 and the sample 1100 of B-doped Si(111) are shown in the bottom panels of Figure 4. Theoretical spectra obtained for different positions of B atoms at or below the reconstructed Si(111) surface (cf. Figure 2) are shown in the upper panels of Figure 4. Lines identified in the legend as Pxy stand for spectra with the polarization vector parallel to the surface (normal incidence), lines identified as Pz stand for spectra with the polarization vector perpendicular to the surface (grazing incidence). One can see that the differences between theoretical spectra for different structural models are large.

When comparing the theory with experiment, one can see that the L_1^c model is by far superior to other structural models, both for the sample 900 and the sample 1100. However, one should also consider that the experimental spectra exhibit significant differences between the samples 900 and 1100. To get a more complete picture, we performed best-fitting of the experimental spectra assuming that the B atoms can be located in various positions simultaneously (see Figure 2). We employed a fitting procedure which uses several criteria for assessing the similarity between the curves, as implemented in the Msspec package^{31,32}. The mutual alignment of the spectra originated from different sites was performed considering the calculated shifts of the energies of the B 1s levels as shown in Tab. II. These shifts were calculated using the final state rule.

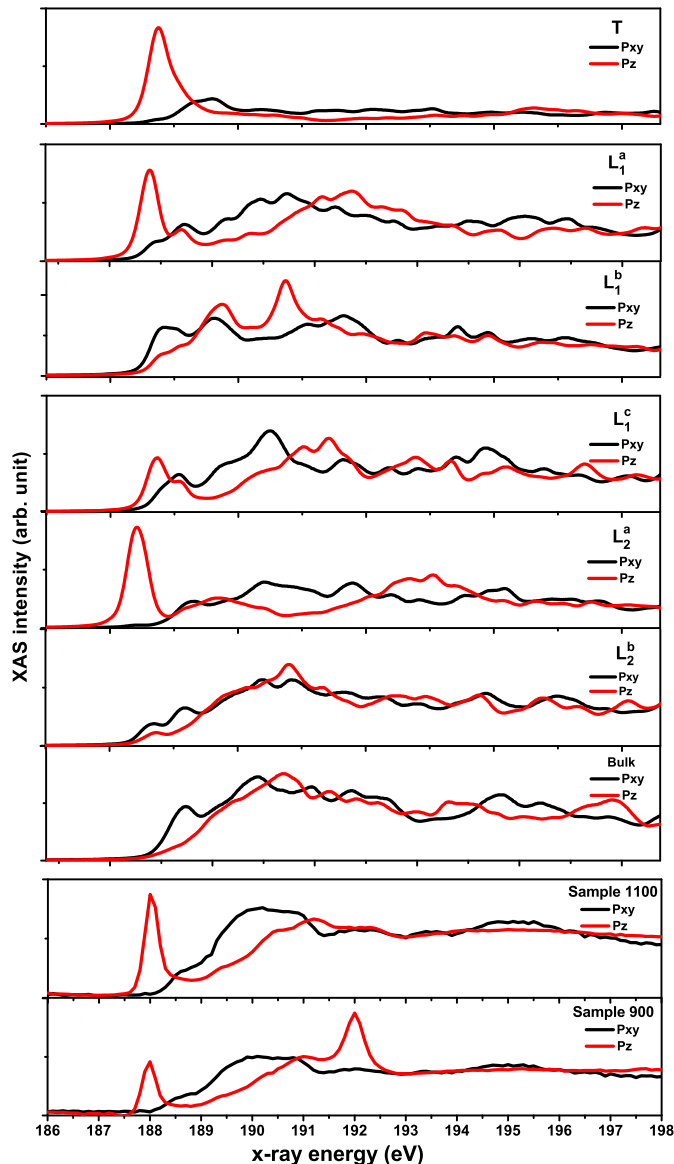


FIG. 4. Polarized B K -edge NEXAFS for B-doped Si(111). Six upper panels show calculated spectra for B atom in different positions denoted in the legend and depicted in Figure 2. Two bottom panels show experimental spectra for the sample 900 and the sample 1100.

TABLE II. Differences between the B $1s$ core level energies for B atoms at different positions as obtained by means of the final state rule. Positive value means that the respective $1s$ electron is bound more strongly than at the L_1^c site.

position	B $1s$ level shift (eV)
L_1^c	0.00
L_2^a	-0.08
L_2^b	0.09
L_1^a	-0.01
L_1^b	0.39
T	0.07
bulk	0.31

A good (though not perfect) fit for the sample 900 is obtained if we assume that 24 % of B atoms are in L_1^a positions and the rest in the L_1^c positions (Figure 5). Concerning the sample 1100, a good fit is obtained by increasing the ratio of B atoms in the L_1^a positions up to 33 % as shown in Figure 5). Considering positions other than L_1^c or L_1^a does not improve the agreement between theory and experiment. As a whole, we conclude that the majority of B atoms occupies the L_1^c position but a sizable portion of them is sitting also somewhere else, possibly in the L_1^a position.

Recently it was suggested that for the L_1^c geometry there may be also some larger B-Si distances present if two-electron bound states are formed in the system³³. We checked that considering such geometry (with the atop Si higher above the B atom than what is shown in figure 3) has no significant effect on the calculated spectra.

IV. DISCUSSION

The main goal of the present work was to find the positions of B atoms at the Si(111) surface depending on the sample preparation techniques. By comparing experimental NEXAFS B K -edge spectra to spectra calculated for various model structures we found that the B atoms

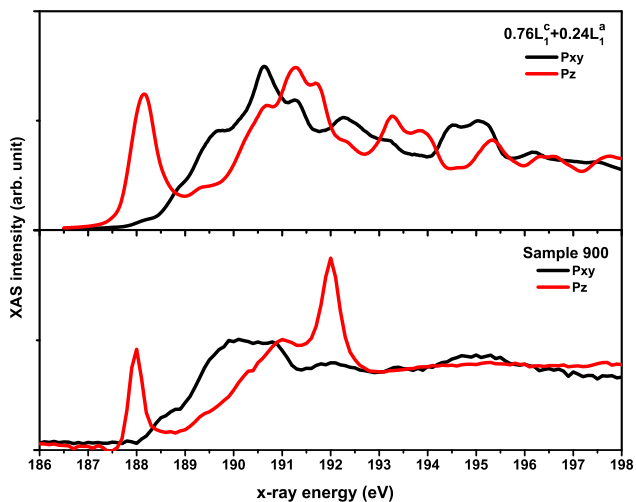


FIG. 5. Experimental B K -edge NEXAFS of the sample 900 compared to theoretical NEXAFS for 76 % of B atoms in L_1^c positions and 24 % of B atoms in L_1^a positions.

are mostly in the L_1^c positions. However, depending on the preparation method, a significant portion of the B atoms appears to be in different locations, first of all in the L_1^a position.

The positions of B atoms as deduced from the NEXAFS experiment agree only partially with the total energies calculations. Most B atoms are located in the L_1^c sites which are also the sites with the lowest total energy (Tab. I). However, the second- and third-lowest energy positions, namely, L_2^a and L_2^b , are not among the sites suggested by the best-fitting procedure. The flashing of the sample used to drive the B atoms from the bulk to the surface is apparently a complex non-equilibrium procedure and may lead to having the B atoms in metastable positions.

Our NEXAFS-based method is complementary to LEED and STM studies. This is because with STM studies one can cover always only a small part of the sample so it is conceivable that in other parts of the sample the sit-

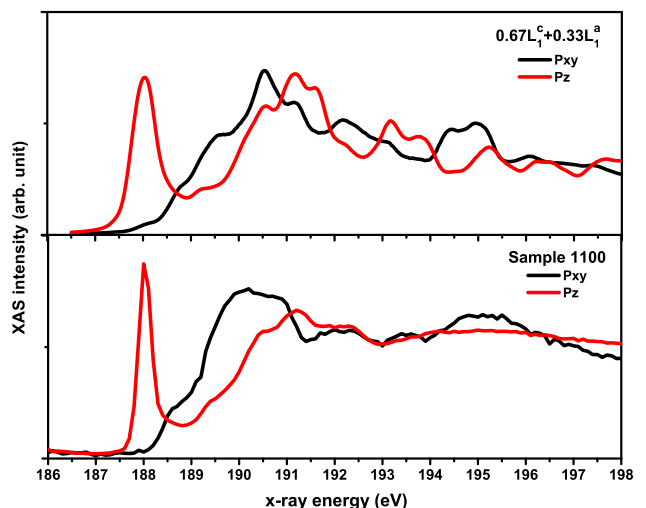


FIG. 6. Experimental B K -edge NEXAFS of the sample 1100 compared to theoretical NEXAFS for 67 % of B atoms in L_1^c positions and 33 % of B atoms in L_1^a positions.

uation may be different than in the part that is studied. X-ray absorption spectroscopy and LEED probe much larger parts of samples so one gets an averaged information concerning the whole system. At the same time, unlike LEED, the x-ray absorption spectroscopy provides a local information because of its chemical specificity.

Similar to our conclusions, few earlier studies also found that some B atoms are located in other than L_1^c positions and that this depends on the heat treatment^{13,16,17}. The exact location of these non- L_1^c boron atoms is not quite clear and it may further differ from sample to sample. Our results indicate that for the sample 1100 which was subject to flashing at 1100 °C, some B atoms might be at the L_1^a sites. However, the agreement between the experiment and the theory for the sample 1100 is worse than for the sample 900 — cf. figures 5 and 6 — so our determination of B atoms positions for the sample 1100 can be regarded as tentative.

The calculations predict big differences between NEXAFS spectra generated for B atoms in different positions — see figure 2. Therefore our conclusions concerning the fact that it is unlikely that a significant portion of B atoms would be in the L_1^b , T, L_2^b and L_2^a positions are quite robust. Reckoning all this, it is possible that some B atoms in the sample 900 might be associated with surface defects¹⁵ or other positions not inspected in this work.

V. CONCLUSIONS

Different preparation conditions of B/Si(111) leads to different positions of B atoms at the surface. Chemically-specific NEXAFS measurements indicate that most of B atoms are in the L_1^c positions, as it follows also from ab-initio calculations of total energies. However, for certain preparation conditions and, in particular, certain modes of heat treatment, a significant portion of B atoms are in other positions. A possible candidate for this other position is the L_1^a position — next to those Si atoms which form the $(\sqrt{3} \times \sqrt{3})R30^\circ$ reconstruction.

ACKNOWLEDGMENTS

We would like to acknowledge projects CEDAMNF (CZ.02.1.01/0.0/0.0/15_003/0000358), LM2015088 and LO1409 of the Ministry of Education, Youth and Sports (Czech Republic).

Appendix A: Core hole effect

We investigate theoretical spectra for the L_1^c structure for different ways of including the core hole to see how this influences the resulting spectra and, based on this, to decide which model is most suitable for our study. The calculated B K-edge NEXAFS spectra of B/Si(111) with no core hole, with half core hole and with a full core hole are shown in Figure 7. One can see that by varying the

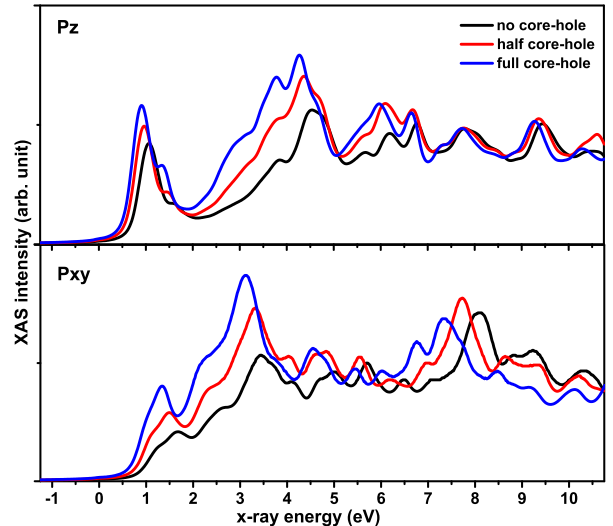


FIG. 7. Influence of the core hole on the B K -edge x-ray absorption spectra of B/Si(111).

strength of the core hole, no new spectral features appear or disappear for spectra with the polarization vector perpendicular to the surface (lines denoted as Pz). However for spectra with the polarization vector parallel to the surface (lines denoted as Pxy), an extra peak appears near the absorption edge if the strength of the core hole increases. Generally, including the core hole leads to an increase of the intensity of peaks close to the absorption edge. Besides, a slight shift of peak positions towards lower energies can be observed.

The full core hole gives the best agreement with experiment for the sample 900 — compare Figures 4 and 7. Therefore we perform all our calculations using this model. At the same time, we are aware that our treatment of the core hole is not perfect and one can expect that including the core hole in a more elaborate way (beyond the static model) would probably lead to better

results. For the purpose of distinguishing between struc-

tural models our treatment of the core hole is, nevertheless, sufficient.

-
- ¹ I. W. Lyo, E. Kaxiras, and P. Avouris, Phys. Rev. Lett. **63**, 1261 (1989).
- ² R. L. Headrick, I. K. Robinson, E. Vlieg, and L. C. Feldman, Phys. Rev. Lett. **63**, 1253 (1989).
- ³ R. G. A. Veiga, R. H. Miwa, and A. B. McLean, Phys. Rev. B **93**, 115301 (2016).
- ⁴ K. Akimoto, I. Hirsawa, T. Tatsumi, H. Hirayama, J. Mizuki, and J. Matsui, Appl. Physics Lett. **56**, 1225 (1990).
- ⁵ H. Huang, S. Y. Tong, J. Quinn, and F. Jona, Phys. Rev. B **41**, 3276 (1990).
- ⁶ P. Baumgärtel, J. J. Paggel, M. Hasselblatt, K. Horn, V. Fernandez, O. Schaff, J. H. Weaver, and A. M. Bradshaw, Phys. Rev. B **59**, 13014 (1999).
- ⁷ P. Bedrossian, R. D. Meade, K. Mortensen, D. M. Chen, J. A. Golovchenko, and D. Vanderbilt, Phys. Rev. Lett. **63**, 1257 (1989).
- ⁸ E. Kaxiras, K. C. Pandey, F. J. Himpsel, and R. M. Tromp, Phys. Rev. B **41**, 1262 (1990).
- ⁹ J. Chang and M. J. Stott, phys. stat. sol. (b) **200**, 481 (1997).
- ¹⁰ H. Q. Shi, M. W. Radny, and P. V. Smith, Phys. Rev. B **66**, 085329 (2002).
- ¹¹ D. P. Andrade, R. H. Miwa, B. Drevniok, P. Drage, and A. B. McLean, J. Phys.: Condens. Matter **27**, 125001 (2015).
- ¹² T. C. Shen, C. Wang, J. W. Lyding, and J. R. Tucker, Phys. Rev. B **50**, 7453 (1994).
- ¹³ A. V. Zotov, M. A. Kulakov, S. V. Ryzhkov, A. A. Saranin, V. G. Lifshits, B. Bullemer, and I. Eisele, Surf. Sci. **345**, 313 (1996).
- ¹⁴ T. Stimpel, J. Schulze, H. E. Hoster, I. Eisele, and H. Baumgärtner, Appl. Surf. Sci. **162**, 384 (2000).
- ¹⁵ E. J. Spadafora, J. Berger, P. Mutombo, M. Telychko, M. Švec, Z. Majzik, A. B. McLean, and P. Jelínek, J. Phys. Chem. C **118**, 15744 (2014).
- ¹⁶ K. Nakamura, K. Masuda, and Y. Shigeta, Surface Science **454–456**, 21 (2000).
- ¹⁷ J. Krügener, H. J. Osten, and A. Fissel, Phys. Rev. B **83**, 205303 (2011).
- ¹⁸ D. Eom, C.-Y. Moon, and J.-Y. Koo, Nano Letters **15**, 398 (2015).
- ¹⁹ S. Tang, A. J. Freeman, and B. Delley, Phys. Rev. B **45**, 1776 (1992).
- ²⁰ M. Ramamoorthy, E. L. Briggs, and J. Bernholc, Phys. Rev. B **59**, 4813 (1999).
- ²¹ A. Sweetman, S. Jarvis, R. Danza, J. Bamidele, S. Gangopadhyay, G. A. Shaw, L. Kantorovich, and P. Moriarty, Phys. Rev. Lett. **106**, 136101 (2011).
- ²² Vasina, Nucl. Inst. Methods A **467–468**, 561 (2001).
- ²³ P. Blaha, K. Schwarz, G. K. H. Madsen, D. Kvasnicka, and J. Luitz, *Wien2k, An Augmented Plane Wave plus Local orbital Program for Calculating the Crystal Properties*, <http://www.wien2k.at> (2001).
- ²⁴ J. P. Perdew, K. Burke, and M. Ernzerhof, Phys. Rev. Lett. **77**, 3865 (1996).
- ²⁵ J. Sun, A. Ruzsinszky, and J. P. Perdew, Phys. Rev. Lett. **115**, 036402 (2015).
- ²⁶ F. Tran, J. Stelzl, and P. Blaha, J. Chem. Phys. **144**, 204120 (2016).
- ²⁷ H. J. Monkhorst and J. D. Pack, Phys. Rev. B **13**, 5188 (1976).
- ²⁸ F. Mandl, *Quantum Mechanics* (Wiley, Chichester, 1992).
- ²⁹ O. Šipr and F. Rocca, J. Synchr. Rad. **17**, 367 (2010).
- ³⁰ U. von Barth and G. Grossmann, Phys. Rev. B **25**, 5150 (1982).
- ³¹ D. Sébilleau, C. Natoli, G. M. Gavaza, H. Zhao, F. D. Pieve, and K. Hatada, Comp. Phys. Commun. **182**, 2567 (2011).
- ³² D. Sébilleau, *The MSSPEC code*, <https://ipr.univ-rennes1.fr/msspec?lang=en> (2017).
- ³³ D. Eom, C.-Y. Moon, and J.-Y. Koo, Nano Letters **15**, 398 (2015), pMID: 25558914.